Theory and operation of a robust controller for a compact adaptive optics system

Benjamin West Frazier, MEMBER SPIE
Xinetics, Inc.
115 Jackson Road
Devens, Massachusetts 01432

Robert K. Tyson, FELLOW SPIE
University of North Carolina at Charlotte
Department of Physics and Optical Science
9201 University City Boulevard
Charlotte, North Carolina 28223
E-mail: rtyson@uncc.edu

Mark Smith
Jacqueline Roche
Xinetics, Inc.
115 Jackson Road
Devens, Massachusetts 01432

Abstract. We describe the design and operation of a high-speed adaptive optics system using a robust H_∞ controller. The system is also general purpose—it can be used in almost any application with minimal modifications and can be set up and operated by a minimally trained operator. The demonstrated system uses a wavefront sensor camera operating at 955 frames/s, a Xinetics 37-channel deformable mirror, and a dual processor computer to perform computations. The system exhibits control of up to 5 waves of focus, a closed-loop bandwidth of ~50 Hz, with a residual error of λ/75 rms. [DOI: 10.1117/1.1814768]

Subject terms: adaptive optics; phase compensation; optical systems; electro-optics.

Paper 030545 received Oct. 30, 2004; revised manuscript received Mar. 10, 2004; accepted for publication Mar. 10, 2004.

1 Introduction

We describe an adaptive optics control system that is being used in a compact, general-purpose system. There were two principal driving requirements: we anticipated a large dynamic range of wavefront errors and we required the operational closed-loop bandwidth to be at least 50 Hz. To reduce the system cost, we chose to use off-the-shelf components and, to improve stability, we chose to incorporate a robust controller rather than a conventional optimal controller. We believe that this is the first application of an H_∞ controller in an adaptive optics system.

In order to design a robust, compact adaptive optics system, it was necessary to incorporate some concepts from modern control theory into a real-time system and lab demonstration. With the extensive amount of literature available on modern optimal control, this becomes a matter of applying the theory to specific problems.

In recent years, a theoretical framework known as H_∞ control has been developed, which allows us to optimize the robustness of a system in the face of uncertainties. The H_∞ method takes a ''worst-case'' approach and provides an upper bound on the system rather than a guaranteed minimum. The design procedure consists of first parameterizing the family of controllers that stabilizes the system and then finding a controller such that the ∞ norm of the system sensitivity is made smaller than some constant, γ. The H_∞ control, in a ''minimax'' sense, serves to minimize the maximum gain of the system.

The H_∞ control theory presented in the literature is highly mathematical in nature, so we adopt an operator approach to control theory. The ''black box'' representation of a system can be thought of as a mathematical operator or a transformation from one normed linear space to another normed linear space. In this framework, signals are vectors and systems are matrices (operators). There is a wealth of knowledge to draw upon from operator theory and functional analysis, and by utilizing abstract mathematics we can develop a generalized theory that is applicable to any adaptive optics system.

The system described here uses a 37-actuator deformable mirror with a separate tip/tilt mirror and controller to alleviate stroke requirements on the deformable mirror. It is designed to operate with closed-loop bandwidth of 50 Hz and requires the use of a high-speed (955 frames/s) wavefront sensor camera.

2 Adaptive Optics Control

2.1 *Limitations of a Classical Decoupled Linear Controller*

The control law for an adaptive optics system can be thought of as a regulator system where it is desired to have the deformable mirror drive all the aberrations to zero. The block diagram of an adaptive optics control system is shown in Fig. 1, which shows the standard feedback arrangement with a deformable mirror, a wavefront sensor, and controller. The input optical aberration is modeled as disturbance noise injected into the system. The surface of the deformable mirror acts as a summing junction for the commands and aberrations and is primarily characterized by its influence matrix. The stiffness of Xinetics PMN actuators along with precision assembly enables the deformable mirror to behave like a linear system.

The system to be controlled is an optical beam so, due to the fact that there is no input-output transfer function associated with the beam itself, there are no dynamics and, consequently, no memory. Memory is generally induced into the system by placing an integrator around the commands, effectively providing a servo loop around the deformable mirror and artificially introducing dynamics, so that the adaptive optics system model can be represented by the state-space equation:

$$\mathbf{x}_{k+1} = \mathbf{x}_k + \mathbf{B}\mathbf{u}_k \tag{1}$$

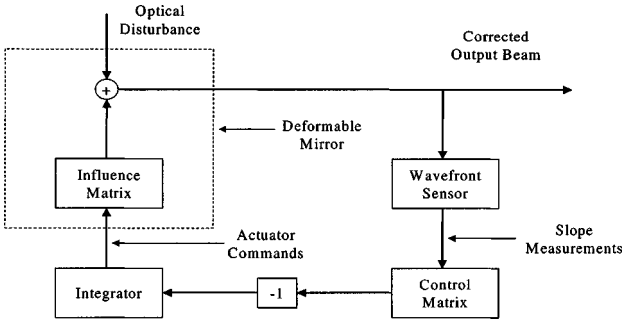

Fig. 1 Controller block diagram for the adaptive optics control loop.

where $\mathbf{x}_k$ is the measured aberration vector at time k, $\mathbf{B}$ is the deformable mirror influence matrix, and $\mathbf{u}_k$ is the command vector at time k.

The concepts of controllability and observability that apply to the deformable mirror and wavefront sensor are discussed elsewhere.[1] These are two important characteristics of control systems because they tell us which modes we can correct with the deformable mirror and which modes we can see with the wavefront sensor.

The most practical method for control is to combine the reconstructor into the controller matrix, so that we perform the wavefront reconstruction indirectly. If we assume that the actuator responses are a linear combination of the slope measurements, we can build this combined reconstructor/controller matrix, providing us with a least squares controller.

The first step is to build the influence matrix $\mathbf{B}$ (often called the geometry matrix[2]) that represents how the actuator commands $\mathbf{u}$ affect the measured slope values or spot location deviations s. During calibration we build the columns of $\mathbf{B}$ by sending each actuator a command independently and then measuring the change in spot positions. Therefore each column of $\mathbf{B}$ represents the range space of its corresponding actuator, or defines the controllability region of each actuator.

$$\begin{pmatrix} s_{1x} \\ s_{1y} \\ \vdots \\ s_{Nx} \\ s_{Ny} \end{pmatrix} = \mathbf{B} \begin{pmatrix} \mathbf{u}_1 \\ \vdots \\ \mathbf{u}_N \end{pmatrix}. \tag{2}$$

To find the reconstructor, we invert $\mathbf{B}$. Since $\mathbf{B}$ is generally not a square matrix, we take the pseudo inverse of $\mathbf{B}$, or $\mathbf{B}^{-1} = (\mathbf{B}\mathbf{B}^T)^{-1}\mathbf{B}^T$. Once we have the reconstructor, we can calculate actuator commands from the matrix-vector product,

$$\begin{pmatrix} \mathbf{u}_1 \\ \vdots \\ \mathbf{u}_N \end{pmatrix} = \mathbf{B}^{-1} \begin{pmatrix} s_{1x} \\ s_{1y} \\ \vdots \\ s_{Nx} \\ s_{Ny} \end{pmatrix}. \tag{3}$$

It is also common to add a row of 1's to the bottom of the $\mathbf{B}$ matrix so that we prevent singularities that arise from the piston component of the wavefront.[3] This extra element can be dealt with by including a 0 in the bottom row of the slope measurement vector to counteract the piston value. This method prevents some problems in calculating the reconstructor.

$$\begin{pmatrix} \mathbf{u}_1 \\ \vdots \\ \mathbf{u}_N \end{pmatrix} = \mathbf{B}^{-1} \begin{pmatrix} s_{1x} \\ s_{1y} \\ \vdots \\ s_{Nx} \\ s_{Ny} \\ 0 \end{pmatrix}. \tag{4}$$

An optimized version of this method may be found.[4]

Combining the reconstructor and controller alleviates some of the computational issues associated with wavefront reconstruction, but it creates problems in other areas. First, it doesn't address the issue of stability at all. By using this method, we are assuming that the system is well posed and internally stable at all frequencies. At low frequencies this is generally true, however, high-frequency dynamics may cause the system to experience oscillations or even limit cycles.

2.2 *Impetus for a Multivariable Controller*

One of the main problems experienced with designing adaptive optics controllers is the multivariable nature of adaptive optics itself. One can derive a controller for a single channel of the adaptive optics system and then replicate this controller for all the channels of the system.[5] This decoupling generally works well in practice because the modes or zones of the system are independent. However, the effects of the actuators on the surface of the mirror cannot be decoupled. In this case, using a control design method that accounts for the coupling can help us find a controller such that the surface of the mirror forms a better fit to the shape of the wavefront. Thus the need for modern multivariable control design methods[6] such as H_∞.

Much research has been done in the area of optimizing the control design for adaptive optics using modern techniques. Many of these designs use frequency domain or adaptive techniques to optimize the closed-loop bandwidth of the system.[7,8] It has been shown that the level of light incident on the wavefront sensor has a dramatic effect on the optimal bandwidth. This concept was then used to optimize multiple closed loop bandwidths corresponding to the different modes of the wavefront.[9] Adaptive filtering techniques have been applied[10–13] and a predictive controller has been outlined.[14] Other detailed analyses of closed-loop systems are presented elsewhere.[15–19]

3 Concept of H_∞ Control

3.1 *Mathematical Background*

A norm is an extension to the Euclidean concept of length and is a measure of the size of a signal or system inside a signal space. In this sense, the norm of a signal x must satisfy three properties:

i Positive Definiteness: $\|x\| \geq 0$ and $\|x\| = 0 \Leftrightarrow x = 0$

ii Homogeneity: $\|\alpha x\| = |\alpha| \|x\|$

iii Triangle Inequality: $\|x+y\| \leq \|x\| + \|y\|$.

A system norm can be thought of as a matrix norm, or a norm induced by a signal norm. In fact, the induced system norms are defined in terms of the behavior of a system as an operator between its normed domain and range spaces.[20]

The two system norms we will be dealing with are $p = 2,\infty$

$$\|A\|_2 := \sqrt{\lambda \max(A^*A)} \tag{5}$$

$$\|A\|_\infty := \max_{1 \leq i \leq n} \sum_{j=1}^{n} |a_{ij}| \quad \text{(Row Sum)}. \tag{6}$$

Signal and system norms are important in operator-based control theory, as these are the parameters we wish to minimize. We can think of the 2 norm as the energy of a signal or system and the ∞ norm as the maximum gain.

Generally, we can treat signals as functions and it is convenient to define spaces of these signals. One of the main purposes of the theory of signal spaces is that we are able to extend the concepts of vector spaces to describe collections of signals or signal spaces. An issue that arises in control theory is that transfer functions that have discontinuities at their poles are not analytic in the neighborhoods surrounding these poles. We can circumvent this problem by mapping certain signal spaces into Hardy spaces.

L_∞ is a normed space consisting of all bounded matrix-valued functions $f(t)$, where the induced norm is given by:

$$\|f\|_\infty := \text{ess} \sup_{\omega \in \mathbb{R}} \overline{\sigma}[\mathbf{F}(j\omega)]. \tag{7}$$

Here, $\overline{\sigma}$ represents the maximum singular value, $\mathbf{F}(j\omega)$ represents the Fourier transform of $f(t)$, and ess sup stands for the essential supremum (least upper bound).

To map the L_∞ spaces into Hardy spaces, we make use of the isomorphic property of the Laplace transform. We start by defining the following orthogonal projections of L_∞:

$$L_\infty^+ = L_\infty[0,\infty)$$
$$L_\infty^- = L_\infty(-\infty,0] \tag{8}$$

where $L_\infty = L_\infty^+ \oplus L_\infty^-$ in the time domain and $L_\infty = H_\infty \oplus H_\infty^\perp$ in the frequency domain. Here, H_∞ is the space of matrix functions $\mathbf{F}(s)$, which are analytic in the open right half plane $[\text{Re}(s)>0]$, and $H_\infty^\perp$ is the space of matrix functions $\mathbf{F}(s)$, which are analytic in the open left half plane $[\text{Re}(s)<0]$. With these definitions, H_∞ can have no poles in the open right half plane and therefore consists of proper and stable rational transfer functions.

In both of these spaces, the induced norm is defined as

$$\|\mathbf{F}\|_\infty = \sup_{\text{Re}(s)>0} \overline{\sigma}[\mathbf{F}(s)], \tag{9}$$

which is the same as the induced norm for the L_∞ space [Eq. (7)]. The Hardy space H_∞ consists of signals and systems with finite energy that are internally stable. In other words, if we force our system to be in this space, we are guaranteed to have a stable system. This is the fundamental concept of H_∞ control.

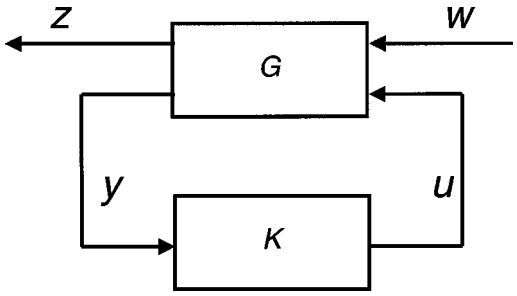

Fig. 2 Transfer function block diagram. The input is *w* and the output is *z*. The state space system is *G* and the state space controller is *K*.

One problem that arises when working with H_∞ control is that a signal space defined by the ∞ norm is convex but not strictly convex, which means there is no guarantee of a unique solution as there is when working with least squares techniques. Therefore, H_∞ control puts an upper bound on system error by seeking a suboptimal controller, i.e., one that is only close to optimal, not precisely optimal.

In addition to the theory of Hardy spaces, an understanding of Lyapunov equations and Riccati equations is essential to modern optimal control. These concepts are fully treated elsewhere.[20,21]

Before we specifically examine H_∞ control, we introduce a notational concept. Packed matrix notation is a compact way for us to represent state-space systems. For example, the system $\mathbf{G}$ with state-space realization:

$$\begin{aligned} \mathbf{x}_{k+1} &= \mathbf{A}\mathbf{x}_k + \mathbf{B}\mathbf{u}_k \\ \mathbf{y}_k &= \mathbf{C}\mathbf{x}_k + \mathbf{D}\mathbf{u}_k \end{aligned} \quad \text{or} \quad \begin{pmatrix} \mathbf{x}_{k+1} \\ \mathbf{y}_k \end{pmatrix} = \begin{pmatrix} \mathbf{A} & \mathbf{B} \\ \mathbf{C} & \mathbf{D} \end{pmatrix} \begin{pmatrix} \mathbf{x}_k \\ \mathbf{u}_k \end{pmatrix} \tag{10}$$

can be represented as:

$$\mathbf{G} = \begin{pmatrix} \mathbf{A} & \mathbf{B} \\ \mathbf{C} & \mathbf{D} \end{pmatrix}. \tag{11}$$

This notation has benefits both for state-space and transfer function representation, as it can easily be presented in the transfer function form as:

$$\mathbf{G}(s) = \mathbf{C}(s\mathbf{I} - \mathbf{A})^{-1}\mathbf{B} + \mathbf{D}. \tag{12}$$

3.2 *Parameterization of Stabilizing Controllers*

Controller parameterization amounts to finding the family of admissible controllers that stabilizes the system. To understand how the controller fits into the system, the generalized feedback structure used in H_∞ control system design approaches is presented in Fig. 2 and the variables are defined as:

w, exogenous inputs: noise, disturbances, and reference commands
z, exogenous output
y, feedback signal
u, control action

G, generalized plant model
K, controller.

From Fig. 2 we can write the augmented state space equations:

$$\mathbf{x}_{k+1}=\mathbf{A}\mathbf{x}_k+(\mathbf{B}_1\mathbf{B}_2)\begin{pmatrix}\mathbf{w}_k\\ \mathbf{u}_k\end{pmatrix}\begin{pmatrix}\mathbf{z}_k\\ \mathbf{y}_k\end{pmatrix}=\begin{pmatrix}\mathbf{C}_1\\ \mathbf{C}_2\end{pmatrix}\mathbf{x}_k+\begin{pmatrix}\mathbf{D}_{11} & \mathbf{D}_{12}\\ \mathbf{D}_{21} & \mathbf{D}_{22}\end{pmatrix}\begin{pmatrix}\mathbf{w}_k\\ \mathbf{u}_k\end{pmatrix} \tag{13}$$

and we can write a packed matrix representation of the system $\mathbf{G}$:

$$\mathbf{G}=\begin{pmatrix}\mathbf{A} & \mathbf{B}_1 & \mathbf{B}_2\\ \mathbf{C}_1 & \mathbf{D}_{11} & \mathbf{D}_{12}\\ \mathbf{C}_2 & \mathbf{D}_{21} & \mathbf{D}_{22}\end{pmatrix}=\begin{pmatrix}\mathbf{G}_{11} & \mathbf{G}_{12}\\ \mathbf{G}_{21} & \mathbf{G}_{22}\end{pmatrix}. \tag{14}$$

Utilizing the method of coprime factorization,[20] we can state the Youla or Q parameterization of stabilizing controllers: Let $\mathbf{G}_{22}=\mathbf{N}\mathbf{M}^{-1}=\tilde{\mathbf{M}}^{-1}\tilde{\mathbf{N}}$ be the right and left coprime factorizations of $\mathbf{G}_{22}$ over H_∞, respectively. Then the set of all proper controllers $\mathbf{K}$ achieving internal stability is parameterized by either $\mathbf{Q}_r$ or $\mathbf{Q}_l\in H_\infty$:

$$\mathbf{K}=(\mathbf{U}_o+\mathbf{M}\mathbf{Q}_r)(\mathbf{V}_o+\mathbf{N}\mathbf{Q}_r)^{-1}=(\tilde{\mathbf{V}}_o+\mathbf{Q}_l\tilde{\mathbf{N}})^{-1}(\tilde{\mathbf{U}}_o+\mathbf{Q}_l\tilde{\mathbf{M}}) \tag{15}$$

provided that the inverses $(\mathbf{V}_o+\mathbf{N}\mathbf{Q}_r)^{-1}$ and $(\tilde{\mathbf{V}}_o+\mathbf{Q}_l\tilde{\mathbf{N}})^{-1}$ exist. Furthermore, the matrices $\mathbf{U}_o$, $\tilde{\mathbf{U}}_o$, $\mathbf{V}_o$, $\tilde{\mathbf{V}}_o\in H_\infty$ and satisfy the Bezout identities:

$$\tilde{\mathbf{V}}_o\mathbf{M}-\tilde{\mathbf{U}}_o\mathbf{N}=\mathbf{I} \quad \text{and} \quad \tilde{\mathbf{M}}\mathbf{V}_o-\tilde{\mathbf{N}}\mathbf{U}_o=\mathbf{I}. \tag{16}$$

Equation (15) provides us with a classification of all the stabilizing controllers for a given plant.

3.3 *H_∞ Synthesis*

The H_∞ control problem is motivated by the desire to minimize the maximum gain of the system. We can state the H_∞ control problem as follows: Given a nominal state space system $\mathbf{G}$, and some $\gamma>0$, find all admissible state space controllers K, which internally stabilize $\mathbf{G}$ such that $\|S(\mathbf{G},\mathbf{K})\|_\infty<\gamma$ where $S(\mathbf{G},\mathbf{K})$ is the star product and defines the system transfer function, $S(G,K)\coloneqq G_{11}+G_{12}K(I-G_{22}K)^{-1}G_{21}$.

The following synthesis method is known as robust stabilization of coprime factors.[6,20]

Let $\mathbf{D}=0$ and $\mathbf{L}=-\mathbf{Y}\mathbf{C}^*$ where $\mathbf{Y}\geqslant 0$ is the stabilizing solution to:

$$\mathbf{A}\mathbf{Y}+\mathbf{Y}\mathbf{A}^*-\mathbf{Y}\mathbf{C}^*\mathbf{C}\mathbf{Y}+\mathbf{B}\mathbf{B}^*=0. \tag{17}$$

Then $\mathbf{P}=\tilde{\mathbf{M}}^{-1}\tilde{\mathbf{N}}$ is a normalized left coprime factorization and

$$\gamma_{\min}\coloneqq(1-\|[\tilde{\mathbf{N}}\tilde{\mathbf{M}}]\|)^{-1/2}=\frac{1}{\sqrt{1-\lambda_{\max}(\mathbf{Y}\mathbf{Q})}}=\inf_{\mathbf{K}\ Stabilizing}\left\|\begin{pmatrix}\mathbf{K}\\ \mathbf{I}\end{pmatrix}(\mathbf{I}+\mathbf{P}\mathbf{K})^{-1}\tilde{\mathbf{M}}^{-1}\right\|_\infty \tag{18}$$

where $\mathbf{Q}$ is the solution to the following Lyapunov equation:

$$\mathbf{Q}(\mathbf{A}-\mathbf{Y}\mathbf{C}^*\mathbf{C})+(\mathbf{A}-\mathbf{Y}\mathbf{C}^*\mathbf{C})^*\mathbf{Q}+\mathbf{C}^*\mathbf{C}=0. \tag{19}$$

If these conditions hold, then for any $\gamma>\gamma_{\min}$, a stabilizing controller achieving

$$\left\|\begin{pmatrix}\mathbf{K}\\ \mathbf{I}\end{pmatrix}(\mathbf{I}+\mathbf{P}\mathbf{K})^{-1}\tilde{\mathbf{M}}^{-1}\right\|_\infty<\gamma$$

is given by

$$\mathbf{K}=\begin{pmatrix}\mathbf{A}-\mathbf{B}\mathbf{B}^*\mathbf{X}_\infty-\mathbf{Y}\mathbf{C}^*\mathbf{C} & -\mathbf{Y}\mathbf{C}^*\\ -\mathbf{B}^*\mathbf{X}_\infty & 0\end{pmatrix} \tag{20}$$

where

$$\mathbf{X}_\infty=\frac{\gamma^2}{\gamma^2-1}\mathbf{Q}\left(\mathbf{I}-\frac{\gamma^2}{\gamma^2-1}\mathbf{Y}\mathbf{Q}\right)^{-1}. \tag{21}$$

We can use Eqs. (17) through (21) to calculate the H_∞ suboptimal controller. Equation (20) defines the controller complete with a state estimator.

3.4 *Modeling Uncertainty*

Uncertainty is always present in our models because we have incomplete knowledge about the system. The benefit of the H_∞ control approach is that we can take these uncertainties (denoted by Δ) into consideration.

The simplest uncertainties are those about which we have no knowledge, except for the maximum value of the uncertainty in the frequency domain (the ∞ norm). For unstructured uncertainties, we can state that for some $\gamma>0$, $\|\Delta\|_\infty\leqslant\gamma$. Uncertainties that we know a great deal about can be represented using the structured singular value approach.[22]

There are two common configurations used to represent uncertainties: additive uncertainty and multiplicative uncertainty. A block diagram of additive uncertainty is shown in Fig. 3. In this figure, $\mathbf{P}$ represents the nominal plant model and $\mathbf{W_A}$ represents the weighting function used to describe specific characteristics of $\Delta_\mathbf{A}\in H_\infty$. In this case, the uncertain model has the form $\mathbf{P_A}=\mathbf{P}+\mathbf{W_A}\Delta_\mathbf{A}$, where $\mathbf{W_A}$, $\mathbf{W_A}^{-1}\in H_\infty$. Additive uncertainty models unknown dynamics operating in parallel with the system.

In multiplicative uncertainty, the uncertainty is either at the plant input or output, as shown in Fig. 4. Here, $\mathbf{P}$ represents the nominal plant model and $\mathbf{W_M}$ represents the weighting function used for $\Delta_\mathbf{M}\in H_\infty$. In this case, the uncertainty model has the form $\mathbf{P_M}=\mathbf{P}(\mathbf{I}+\mathbf{W_M}\Delta_\mathbf{M})$, where

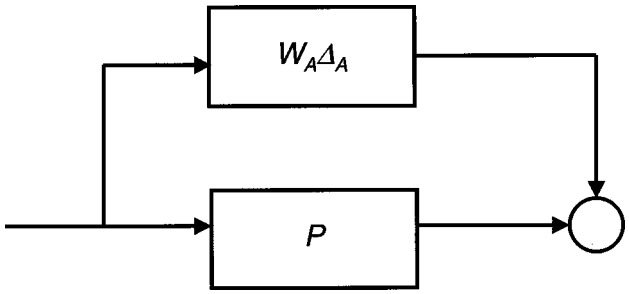

Fig. 3 Block diagram representing additive uncertainty.

$\mathbf{W_M}$, $\mathbf{W_M^{-1}} \in H_\infty$. Multiplicative uncertainty models unknown dynamics operating in series with the plant.

To see how uncertainty affects the system, suppose $\mathbf{M} \in H\infty$ and let $\gamma>0$. Then the interconnected system of Fig. 5 is well posed and internally stable[6,20,21] for all $\Delta(s) \in H_\infty$ with

a. $\|\Delta\|_\infty \leqslant 1/\gamma$ if and only if $\|\mathbf{M}(s)\|_\infty < \gamma$

b. $\|\Delta\|_\infty < 1/\gamma$ if and only if $\|\mathbf{M}(s)\|_\infty \leqslant \gamma$.

The above statement is known as the small gain theorem and it tells us that if we make the ∞ norm of the system small enough, we are guaranteed to have a robustly stable system in spite of any uncertainties that are present. This is a crucial theorem in the development of H_∞ control theory.

The small gain theorem is applicable to Fig. 5 if we define $\mathbf{M}$ as[23]

$$\mathbf{M}=S(\mathbf{P},\mathbf{K})=\begin{pmatrix}\mathbf{M}_{11} & \mathbf{M}_{12}\\ \mathbf{M}_{21} & \mathbf{M}_{22}\end{pmatrix}. \tag{22}$$

3.5 *Uncertainty Applied to Adaptive Optical Systems*

Environmental changes and disturbances play a key role in the performance of any adaptive optical system. Since the control of the deformable mirror depends solely on the influence matrix, which is collected prior to running the system, any changes to the system are not represented in the control algorithm. Because the stroke of the actuators is temperature-dependent, a slight change in temperature causes the performance of the actuators to vary without the influence matrix being updated. In fact, any noise in the system affects both the accuracy of the influence matrix as well as the accuracy of the wavefront measurements and prevents optimal performance when using a least squares fit algorithm.

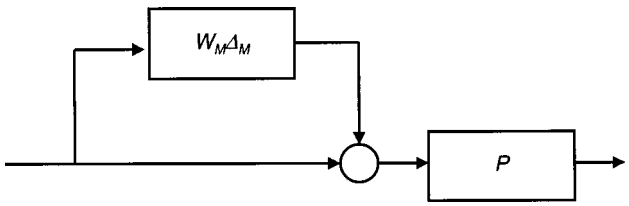

Fig. 4 Block diagram representing multiplicative uncertainty.

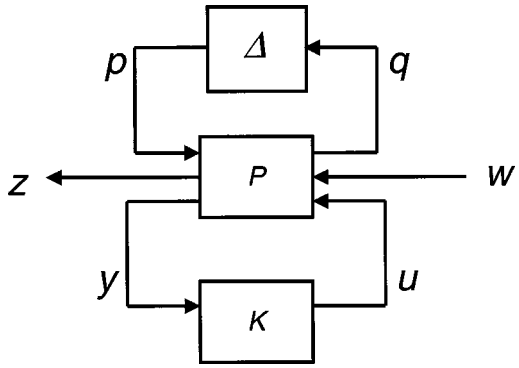

Fig. 5 Transfer function block diagram including noise uncertainty.

The influence matrix is collected using a single command to each actuator. When using a least squares fit to correct wavefront aberrations, the commands are based on the shape of the surface of the mirror scaling linearly. Hence, if the deformable mirror does not have stiff bond joints, or the actuator stroke is not linear, the shape of the surface of the mirror will not scale linearly to the commanded voltages. Therefore, any hysteresis in the actuator or imprecision in assembly will also cause uncertainty in the model. The voltage-stroke transfer function for a typical PMN actuator is displayed in Fig. 6. This figure shows the hysteresis present in an actuator is extremely small, roughly 1% of the nominal value. Precision assembly represents an uncertainty that cannot be quantified.

The uncertainty in an adaptive optical system can be modeled as an input multiplicative unstructured uncertainty containing noise, thermal effects, hysteresis, and coupling in the state transition matrix and is represented by Δ. If we follow the notation of Zhou, Doyle, and Glover[20] and define the input and output sensitivity and complementary sensitivity functions as:

$$\mathbf{S}_0=(\mathbf{I}+\mathbf{PK})^{-1}, \quad \mathbf{T}_0=\mathbf{I}-\mathbf{S}_0 \tag{23}$$

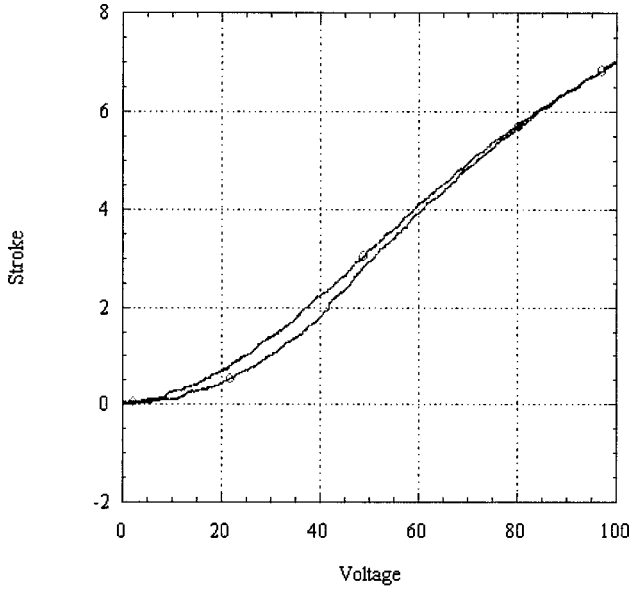

Fig. 6 Voltage-stroke transfer function for a typical PMN actuator.

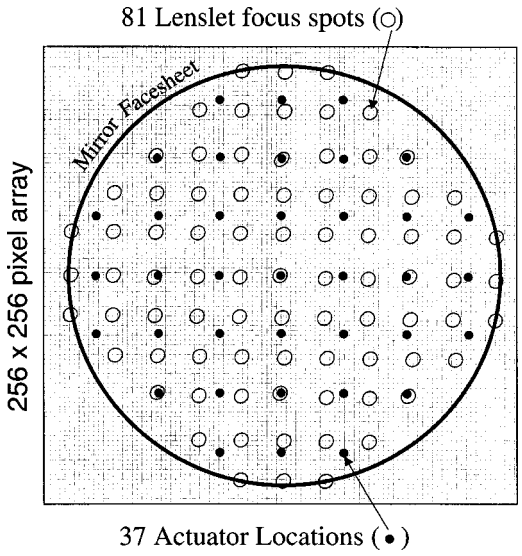

Fig. 7 Relative positions of the 81 wavefront sensor subapertures (lenslet focus spots) and the position of the 37 actuators. The irregular registration between the two subsystems is accommodated during the calibration of the control system and building of the reconstructor.

$$\mathbf{S}_i=(\mathbf{I}+\mathbf{KP})^{-1}, \quad \mathbf{T}_i=\mathbf{I}-\mathbf{S}_i \tag{24}$$

where $\mathbf{K}$ is the internally stabilizing controller for the nominal plant $\mathbf{P}$, and the set of uncertain plants Π is:

$$\Pi=\mathbf{P}(\mathbf{I}+\Delta) \tag{25}$$

we can then define the condition for robust stability of an adaptive optical system as:

$$\|\Delta\|_\infty<\mathbf{1}\text{iff}\|\mathbf{T}_i\|_\infty\leqslant 1. \tag{26}$$

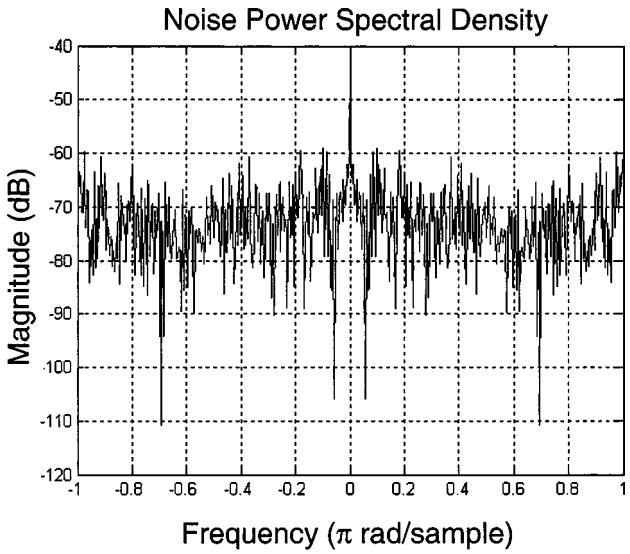

Fig. 8 Power spectral density of the noise including local air turbulence, camera noise, and algorithm errors.

Table 1 Measured noise parameters.

Parameter	Value
$\|\sigma_x\|_2$	4.4473 waves
$\|\sigma_x\|_\infty$	0.0779 waves
Variance	2.8×10^{-4} waves^2
Standard Deviation	0.0148 waves
Mean	−0.0103 waves
Max	0.0508 waves
Min	−0.0779 waves

4 System Implementation

4.1 *Controller Design*

The realization of the suboptimal H_∞ controller is accomplished in a calibration step, as in the least squares methods. The Riccati equations are solved by a Schur eigenvalue decomposition,[20] from which the suboptimal controller itself is found. The actual implementation of the control is accomplished with a series of matrix-vector multiplications to compute the wavefront estimates and then the necessary actuator commands.

4.2 *System Performance*

The adaptive optical system built at Xinetics Inc. has three primary components: a 37-channel deformable mirror, a high-speed wavefront sensor, and a dual processor computer to keep up with the system. The deformable mirror is

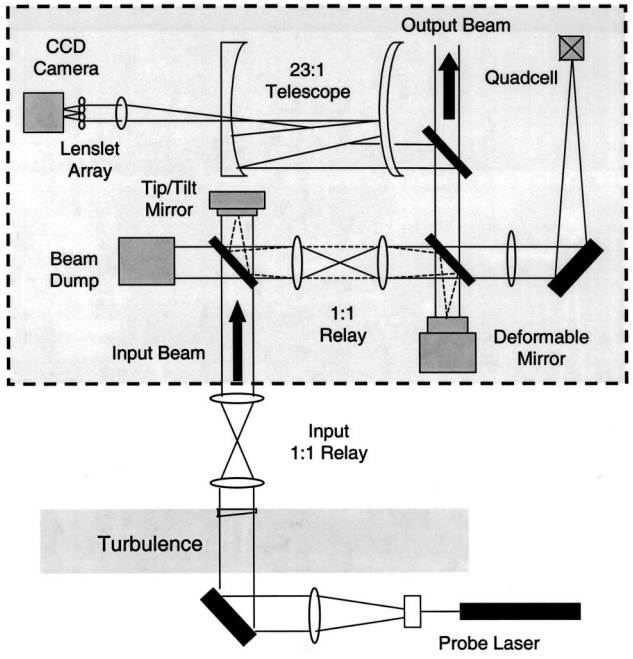

Fig. 9 Adaptive optics system configuration. The system is intended to correct the beam after it experiences aberrating effects from the turbulence. The input and output beam size dictates the 23:1 telescope for insertion into the high-speed CCD camera wavefront sensor. Tip/tilt is corrected independently of the deformable mirror but they are positioned at optical conjugate planes.

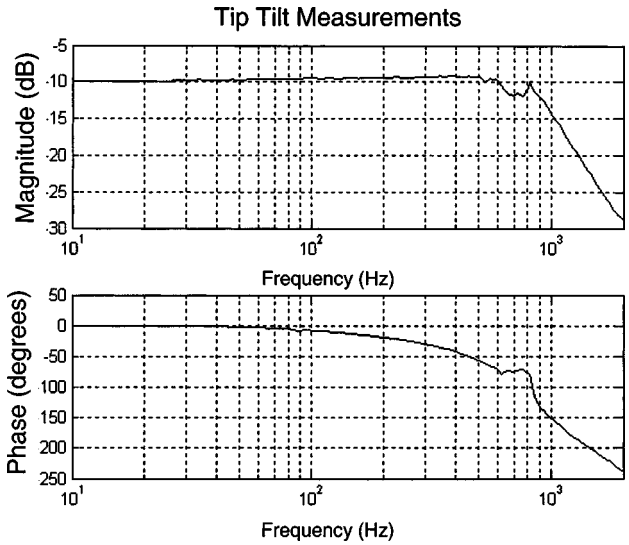

Fig. 10 Experimental open-loop Bode plot of the tip/tilt look indicating an expected 250-Hz closed-loop bandwidth.

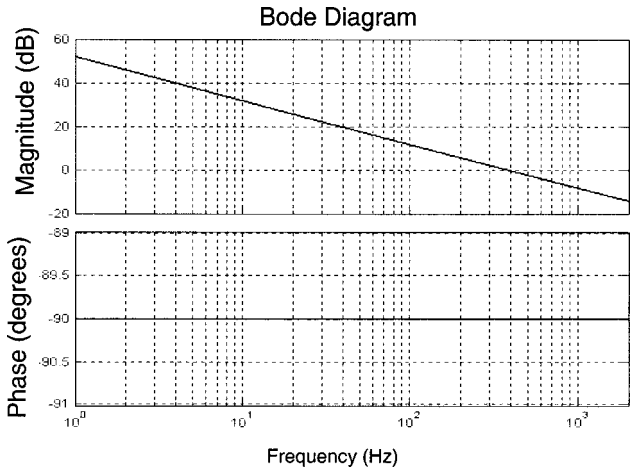

Fig. 11 Theoretical Bode plot of the integrator.

a standard 37-channel discrete actuator design, with 7-mm spacing between the actuators. The wavefront sensor is a Shack-Hartmann sensor. It utilizes a DALSA camera operating at 955 frames/s, with 10-μm pixels in a 256×256 grid, for an active sensor size of 2.5 mm. Also used is a lenslet array with 190-μm pitch and a 10-mm focal length. The setup provides 81 spots over the control aperture. The input beam is a 20-mW HeNe laser, operating at 632.8 nm. The computer uses two Xeon processors running at 3.06 GHz. The use of 81 spots over an aperture with 37 actuators provides a great deal of flexibility in the alignment of the system, as shown in Fig. 7.

Noise floor measurements, shown in Fig. 8, report the power spectral density of the output of the system while running without commanding the deformable mirror. Because the mirror surface remains constant, the noise measured consists only of centroiding algorithm errors, camera noise, and air turbulence. The data is based on 1000 frames, providing 162,000 noise measurements. Several standard statistical parameters are presented in Table 1. Since the sampling rate of the system is 955 Hz, a discrete time frequency of π rad/sample corresponds to a continuous time frequency of 477.5 Hz. The low-noise floor, with a dc noise power of -40 dB, should have a negligible effect on the system. Since this step of the experiment was not run closed-loop, the results do not indicate uncertainty in the system model, only the noise present in the system.

The system (Fig. 9) was designed to have an overall closed-loop control bandwidth of approximately 50 Hz and has repeatedly demonstrated a residual error of 1/75 wave rms.

The verification of the tip/tilt loop was done by experimentally measuring the open-loop frequency response ex-

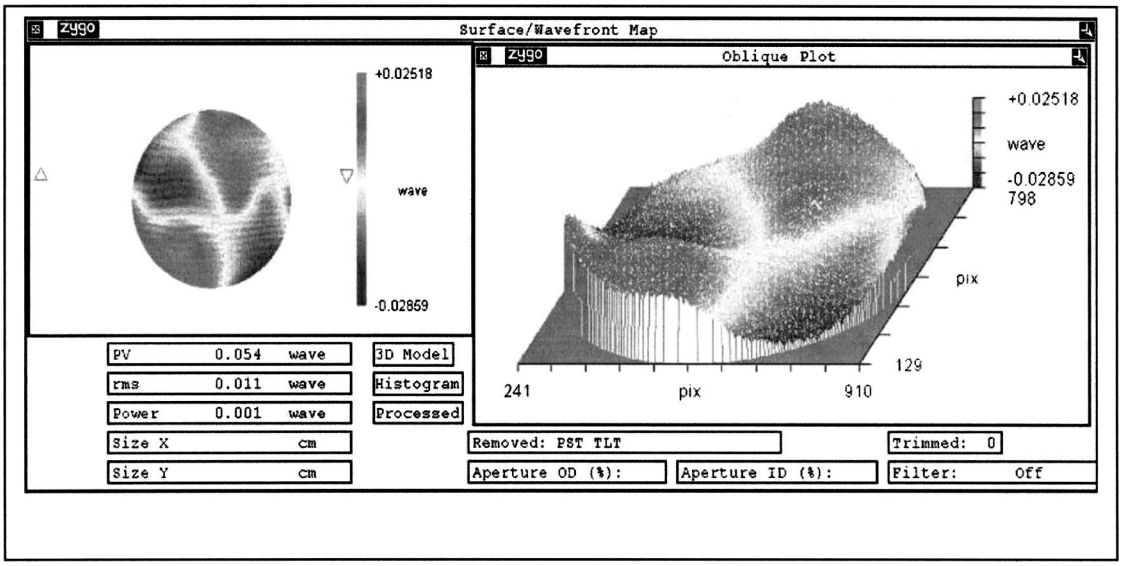

Fig. 12 Screen of the output of the diagnostic interferometer showing a λ/90 rms wavefront residual. Taking further data over various conditions, we never encountered an error worse than λ/75.

cluding the integrator. The experimental open-loop Bode plot is presented in Fig. 10; the theoretical Bode plot of the integrator is presented in Fig. 11. These plots show that the tip/tilt loop has an expected closed loop bandwidth of around 250 Hz.

The residual wavefront error in flattening the mirror was tested using an interferometer. An interferogram was taken while all actuator commands were zero. Then, the system was run in closed-loop operation for 1000 frames. The only input was the combined noise of the local air turbulence, centroiding error, and camera noise.

After running, a second interferogram of the surface of the deformable mirror was taken and subtracted from the original image to determine the residual wavefront error. Over a period of 10 trial runs, the worst observed rms error was 1/75 wave (0.013λ) and the best observed rms error was 1/90 wave (0.011λ), as shown in Fig. 12.

To further evaluate the operation of the system, focus convergence tests were performed. In these tests, a known amount of focus was injected into the system after calibration. An interferogram was taken of the deformable mirror surface after the system ran for a single frame. When the surface of the deformable mirror reached a steady state value, the system was determined to have converged. In repeated tests, the system demonstrated convergence after a single frame, and this convergence rate was seen over the entire five-wave dynamic range of the wavefront sensor. In each case, the steady-state surface error after running the system for 1000 frames remained within 1/75 wave rms.

The fact that the H_∞ controller demonstrated convergence after a single frame for the entire dynamic range of the wavefront sensor signifies it has no performance penalty compared to the standard least squares controller. In addition, no gain attenuation in any of the experiments using the H_∞ controller suggests that the H_∞ controller does indeed provide a more robustly stable system. Finally, while this appears to be the first demonstration of a H_∞ control in an adaptive optics system, the H_∞ is not expected to outperform the least squares controller, but it is expected to be more robustly stable.

References

1. M. E. Furber and D. Jordan, ''Optimal design of wavefront sensors for adaptive optical systems: part 1, controllability and observability analysis,'' *Opt. Eng.* **36**, 1843–1855 (1997).
2. W. J. Wild, ''Innovative wavefront estimators for zonal adaptive optics systems II,'' *Proc. SPIE* **3353**, 1164–1173 (1998).
3. R. K. Tyson, *Introduction to Adaptive Optics*, SPIE Press, Bellingham, WA (2000).
4. E. P. Wallner, ''Optimal wave-front correction using slope measurements,'' *J. Opt. Soc. Am.* **73**, 1771–1776 (1983).
5. J. W. Hardy, *Adaptive Optics for Astronomical Telescopes*, Oxford University Press, New York (1998).
6. J. C. Doyle, K. Glover, P. P. Khargonekar, and B. A. Francis, ''State-space solutions to standard H_2 and H_∞ control problems,'' *IEEE Trans. Autom. Control* **34**, 831–847 (1989).
7. R. T. Brigantic, M. C. Roggemann, B. M. Welsh, and K. W. Bauer, ''Closed loop bandwidth optimization to maximize adaptive optics system performace,'' *Proc. SPIE* **3126**, 151–162 (1997).
8. R. T. Brigantic, M. C. Roggemann, B. M. Welsh, and K. W. Bauer, ''Optimization of adaptive-optics systems closed-loop bandwidth settings to maximize imaging-system performance,'' *Appl. Opt.* **37**, 848–855 (1998).
9. B. L. Ellerbroek, C. Van Loan, N. P. Pitsianis, and R. J. Plemmons, ''Optimizing closed-loop adaptive-optics performance with use of multiple control bandwidths,'' *J. Opt. Soc. Am. A* **11**, 2871–2886 (1994).
10. J. S. Gibson, C. C. Chang, and B. L. Ellerbroek, ''Adaptive reconstructors for adaptive optics,'' *Proc. SPIE* **3706**, 326–337 (1999).
11. J. S. Gibson, C.-C. Chang, and B. L. Ellerbroek, ''Adaptive optics: wave-front correction by use of adaptive filtering and control,'' *Appl. Opt.* **39**, 2525–2538 (2000).
12. E. W. Justh, M. A. Vorontsov, G. W. Carhart, L. A. Beresnev, and P. S. Krishnaprasad, ''Adaptive optics with advanced phase-contrast techniques. II. High-resolution wave-front control,'' *J. Opt. Soc. Am. A* **18**, 1300–1311 (2001).
13. L. Zhu, P.-C. Sun, D.-U. Bartsch, W. R. Freeman, and Y. Fainman, ''Adaptive control of a micromachined continuous-membrane deformable mirror for aberration compensation,'' *Appl. Opt.* **38**, 168–176 (1999).
14. C. Dessenne, P.-Y. Madec, and G. Rousset, ''Optimization of a predictive controller for closed-loop adaptive optics,'' *Appl. Opt.* **37**, 4623–4633 (1998).
15. B. L. Ellerbroek and D. W. Tyler, ''Modeling the combined effect of static and varying phase distortions on the performance of adaptive optical systems,'' *Appl. Opt.* **38**, 3857–3868 (1999).
16. B. L. Ellerbroek, ''Power series evaluation of covariances for turbulence-induced phase distortions including outer scale and servo lag effects,'' *J. Opt. Soc. Am. A* **16**, 533–548 (1999).
17. G. A. Tyler, ''Turbulence-induced adaptive optics performance degradation: evaluation in the time domain,'' *J. Opt. Soc. Am. A* **1**, 251–262 (1984).
18. M. R. Whiteley, B. M. Welsh, and M. C. Roggemann, ''Optimal modal wave-front compensation for anisoplanatism in adaptive optics,'' *J. Opt. Soc. Am. A* **15**, 2097–2106 (1998).
19. V. E. Zuev and V. P. Lukin, ''Dynamic characteristics of optical adaptive systems,'' *Appl. Opt.* **26**, 139–144 (1987).
20. K. Zhou, J. C. Doyle, and K. Glover, *Robust and Optimal Control*, Prentice Hall, New Jersey (1996).
21. G. Dullerud and F. Paganini, *A Course in Robust Control Theory—A Convex Approach*, Springer-Verlag, New York (2000).
22. J. Doyle, ''Analysis of feedback systems with structured uncertainties,'' *Proc. IEEE* **133**, 45–56 (1982).
23. J. Chen and G. Gu, *Control-Oriented System Identification—An H_∞ Approach*, John Wiley & Sons, New York (2000).

Benjamin West Frazier received his BSEE degree and his MSEE degree from the University of North Carolina at Charlotte in 2000 and 2003, respectively. He is currently employed as an associate electrical engineer with Xinetics Inc. in Devens, Massachusetts, where he designs real-time control systems for adaptive optics.

Robert K. Tyson is an associate professor of physics and optical science at the University of North Carolina at Charlotte. He is a fellow of SPIE and he is the author of three books and the editor of ten volumes on adaptive optics. He has a BS from Penn State University and MS and PhD degrees from West Virginia University. His current research interests include atmospheric turbulence studies, classical diffraction, and novel wavefront sensing and amplitude and phase manipulation techniques to enhance propagation, laser communications, and imaging.

Mark Smith received his BS degree in physics from the University of Massachusetts at Lowell in 1986 and has been developing wavefront sensors and adaptive optics systems for the past 20 years. He is currently employed as the director of the Adaptive Optics Group at Xinetics Inc. in Devens, Massachusetts, and oversees design and construction of all wavefront control and driver systems.

Jacqueline Roche received her BS in physics from Center College in Danville, Kentucky, in 1998 and her MSME from the University of Kentucky in 2001. She is currently employed as an associate mechanical engineer with Xinetics Inc. in Devens, Massachusetts, where she works with static adaptive optics optimization and deformable mirror qualification.